Computing Resistivity Anisotropy and Structural Dip Using Multi-component Induction Data

Berthold Kriegshäuser, Bill Corley, Michael Rabinovich, Lev Tabarovsky, Baker Atlas

Abstract

A multi-component induction tool like the 3DEX^{SM} provides all the data necessary to derive formation resistivity parallel and perpendicular to bedding. It has been shown in the past that the resistivity perpendicular to bedding can be extremely important to detect and quantify hydrocarbons in so-called low-resistivity pay zones. However, in order to accurately derive formation resistivities at any relative dip from the 3DEX data, the formation dip and azimuth needs to be known. Until recently, this information needed to be provided as a priori information, either from surface seismic data, and/or derived from borehole imaging analysis. In this paper we discuss a new method that utilizes all 3DEX data to derive not only formation resistivities parallel and perpendicular to bedding but also formation dip and azimuth.
The 3DEX tool is comprised of three mutually orthogonal transmitter-receiver pairs that allow measurement of the full magnetic field matrix at multiple frequencies. Using a rapid two-step least-square optimization scheme we first derive at every logging depth formation dip and azimuth; then we compute formation resistivities parallel and perpendicular to bedding.
We first validated our algorithm with synthetic examples, and then, we applied this enhanced processing to many field data sets, for example, to data acquired offshore Brazil. The generally good agreement between the computed formation dips and azimuths from 3DEX data and those obtained from borehole imaging data confirm the strength and efficacy of this new processing algorithm.

Introduction

The 3DEX^{SM} tool is comprised of three mutually orthogonal transmitter-receiver pairs that measure all nine magnetic field components at multiple frequencies (Kriegshauser et al., 2000, 2001). The instrument operates at 10 different frequencies between 20 and 220 kHz. The main objective for this tool is to improve formation evaluation in thinly laminated reservoirs by measuring the horizontal and vertical resistivities, Rh and Rv, i.e., parallel and perpendicular to bedding (Klein, 1996, Mollison et al., 1999, Schoen et al., 1999). Utilizing Rh and Rv jointly in computing hydrocarbon saturations also reduces uncertainties in estimating hydrocarbon reserves (Mollison et al., 2001).

Previous processing software (Rabinovich & Tabarovsky, 2001; Tabarovsky et al., 2001, Kriegshauser et al., 2001) used only the three main in-line components to invert for Rh and Rv. Formation dip and azimuth in addition to the orientation measurements from a digital orientation tool were provided as an input. Because only the in-line components were used in the processing, the operational envelope of 3DEX was limited to about 50 deg relative dip.

The newly developed algorithm utilizes also the off-diagonal magnetic field components, i.e., cross-components, in the processing. This not only yields formation dip and azimuth, but also improves computation of Rh and Rv, while extending the operational envelope of 3DEX to 75-80 deg relative dip. In close to horizontal wells, a different processing has to be applied (Yu et al., 2004).

The new algorithm was first verified on synthetic data. After initial tests with thick anisotropic layers, we constructed a synthetic data set to simulate the Gulf of Mexico conditions. A 170-m interval included 55 layers with the horizontal resistivities ranging from 0.4 to 20 Ohm-m and an anisotropy ratio from 1 to 5. The relative dip was 59.8°. The tool rotation was fast, and the model included isotropic layers. The recovered formation orientation and resistivities agree well with the parameters of the synthetic model.

Method

The magnetic field measurements made by 3DEX can be described by a 3-by-3 matrix, where the first and second index corresponds to the transmitter and receiver magnetic dipole direction (Figure 1).

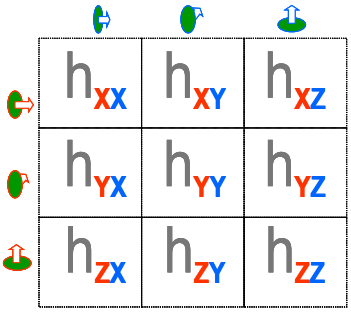

Fig. 1 *Magnetic measurement tensor. The first and second index indicates the orientation of a transmitter and the receiver, respectively.*

The magnetic field tensor, generally, is not symmetric. This means that there may be models and situations when $h_{xy} \neq h_{yx}$, $h_{xz} \neq h_{zx}$, $h_{yz} \neq h_{zy}$ (Figure 2). This demonstrates there is no direct correspondence between the structure of the conductivity tensor and the measurement tensor.

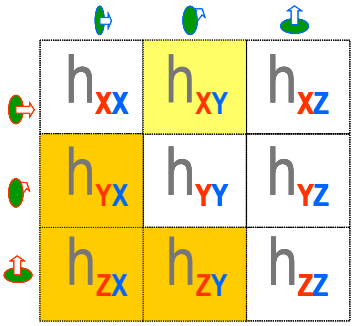

Fig. 2 *Non-symmetric measurement tensor. Generally all 9 components are different.*

Multi-frequency focusing (MFF). The current pattern and the behavior of the corresponding magnetic fields measured by the 3DEX tool are complex, even in a uniform formation. Borehole and invasion can cause additional significant distortions. We have developed a Multi-Frequency Focusing for the 3DEX measurements, MFF, which allows us to eliminate effects of the near borehole zone (Tabarovsky and Rabinovich, 1998; Tabarovsky et al., 2001; Yu et al., 2003).

MFF processing is based on the Taylor expansion of the measured field into a frequency series. The second term of the series does not depend on the borehole and invasion properties. MFF is a mechanism for deriving this term from the multi-frequency measurements. In a resistive formation, two frequencies are sufficient. When only two frequencies are used MFF reduces to a dual frequency approach (Tabarovsky & Epov, 1979). The more conductive the formation, the more terms in the expansion and more frequencies are required to recover the necessary term accurately (Tabarovsky et al., 2001).

PRINCIPAL COMPONENTS AND SEPARATION OF MODES

In the following discussion we consider a layered transverse isotropic formation. For each layer the conductivity tensor in the principal coordinate system is described as

$$\hat{\sigma} = \begin{pmatrix} \sigma_h & & \\ & \sigma_h & \\ & & \sigma_v \end{pmatrix}. \qquad (1)$$

The magnetic field tensor (Fig. 2) in general cannot be diagonalized. However, an additional feature of the MFF transformation is that the MFF-transformed magnetic field measurements from Figure 2 can be diagonalized:

$$\hat{\mathrm{H}}_{MFF} = \begin{pmatrix} \tilde{h}^{p}_{xx} & & \\ & \tilde{h}^{p}_{yy} & \\ & & \tilde{h}^{p}_{zz} \end{pmatrix}. \qquad (2)$$

In this diagonal matrix $\tilde{h}^{p}_{xx} = \tilde{h}^{p}_{yy}$, which is an important feature of the MFF signal that reduces the number of principal components to two.

Knowing the principal components $\tilde{h}^{p}_{xx}$, $\tilde{h}^{p}_{zz}$ and angles θ, φ we can express measured MFF components as

$$\begin{pmatrix} \tilde{h}_{xx} \\ \tilde{h}_{xy} \\ \tilde{h}_{xz} \\ \tilde{h}_{yx} \\ \tilde{h}_{yy} \\ \tilde{h}_{yz} \\ \tilde{h}_{zx} \\ \tilde{h}_{zy} \\ \tilde{h}_{zz} \end{pmatrix} = \begin{pmatrix} c_\varphi^2 c_\theta^2 + s_\varphi^2 & c_\varphi^2 s_\theta^2 \\ c_\varphi s_\varphi - c_\varphi s_\varphi c_\theta^2 & -c_\varphi s_\varphi s_\theta^2 \\ c_\varphi c_\theta s_\theta & -c_\varphi c_\theta s_\theta \\ c_\varphi s_\varphi - c_\varphi s_\varphi c_\theta^2 & -c_\varphi s_\varphi s_\theta^2 \\ s_\varphi^2 c_\theta^2 + c_\varphi^2 & s_\varphi^2 s_\theta^2 \\ -s_\varphi c_\theta s_\theta & s_\varphi c_\theta s_\theta \\ c_\varphi c_\theta s_\theta & -c_\varphi c_\theta s_\theta \\ -s_\varphi c_\theta s_\theta & s_\varphi c_\theta s_\theta \\ s_\theta^2 & c_\theta^2 \end{pmatrix} \begin{pmatrix} \tilde{h}^{p}_{xx} \\ \tilde{h}^{p}_{zz} \end{pmatrix}, \qquad (3)$$

where

$s_\varphi = \sin\varphi,$

$c_\varphi = \cos\varphi,$

$s_\theta = \sin\theta,$

$c_\theta = \cos\theta.$

Note that $\tilde{h}^{p}_{xx}$ depends on both horizontal and vertical conductivity, while $\tilde{h}^{p}_{zz}$ depends only on horizontal conductivity. The over-determined system (Equ. 3) has four unknowns – two angles and two principal components. Knowing the principal components is equivalent to knowing the principal conductivities although it must be noted that inversion is required to extract conductivities from the principal components. We can apply a sequential inversion of the principal components: first extracting the horizontal conductivity from the $\tilde{h}^{p}_{zz}$ component and then fixing horizontal conductivity recover vertical conductivity from $\tilde{h}^{p}_{xx}$ component.

DETERMINATION OF FORMATION DIP AND AZIMUTH

Examining Equation 3 we observe that in the right-hand side we have 4 unknowns $\tilde{h}^{p}_{xx}$, $\tilde{h}^{p}_{zz}$, θ, and φ. Thus, if the tool acquires 4 or more independent components, we can solve this system of equations using a least-square approach. Because Equation 3 is correct at every logging depth, we propose the following algorithm that provides

maximum stability and robustness in recovering the formation dip and azimuth:

- We divide the entire processing intervals into relatively small windows and assume the formation dip and formation azimuth to be constant in every window.
- In each window at each logging depth, we incrementally change the formation dip from zero to ninety degrees.
- For every formation dip we incrementally change the formation azimuth from 0 to 360 degrees.
- Knowing the orientation angles for each formation dip and azimuth pair, we calculate relative angles θ and φ.
- For every θ and φ pair, we solve the system of Equation 3 for the unknowns $\widetilde{h}_{xx}^{p}$, $\widetilde{h}_{zz}^{p}$ using the least-square technique.
- We substitute every four values θ, φ, $\widetilde{h}_{xx}^{p}$, $\widetilde{h}_{zz}^{p}$ into Equation 3 and calculate the misfit value (in χ^2–norm) of the measured MFF components and the calculated values $\widetilde{h}$ from Equation 3.
- For every θ and φ (or for the formation dip and azimuth) pair, we sum the misfits for all logging depths in the window and select the one with the minimum value.
- With the known θ and φ (or the formation dip and azimuth), we calculate $\widetilde{h}_{xx}^{p}$, $\widetilde{h}_{zz}^{p}$ at each depth used in the following sequential interpretation for σ_h and σ_v (Tabarovsky et al., 2001).

3DEX PROCESSING FLOW CHART

A general 3DEX processing flow chart is presented in Figure 3. It consists of two main parts:

- Processing for formation dip and azimuth and two principal components;
- Sequential inversion for Rh and Rv using two principal components.

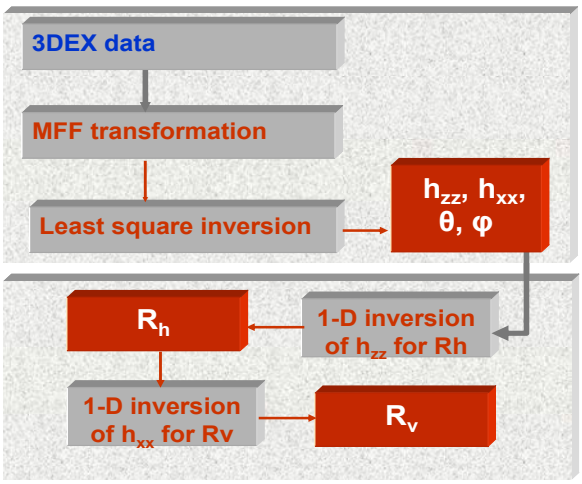

Fig. 3 *3DEX processing flow chart.*

Below we briefly discuss each part in the following sections.

Processing for formation dip and azimuth and two principal components. All measured components are provided as an input. Because theoretically only four components are required for recovering four unknowns, a user has the possibility to exclude some of the components. However, we recommend using all components. Additional components are used to minimize the uncertainties and suppress measurement noise.

An MFF transformation is applied to the measured single frequency data (Tabarovsky and Rabinovich, 1998). There are two main reasons for applying the MFF transformation: elimination of the near borehole effects (Tabarovsky et al., 2001; Yu et al., 2003) and reduction of modes from 5 in single frequency measurements to 2 in multi-frequency (see section “Principal components and separation of modes”).

After applying the MFF transformation, we apply the least-square inversion described in the previous section.

Sequential inversion for Rh and Rv. In multi-parametric inversion it is always preferable to perform optimization sequentially for independent, separable parameters or parametric groups if such parameters or groups exist and can be identified (Tabarovsky and Rabinovich, 1998). This is especially important if the measurements have essentially different sensitivity to different parameters. If we try to invert for these parameters simultaneously, small errors in parameters of high importance (to which data is sensitive) will cause big errors in parameters of low importance (to which data is not sensitive).

It is well known that the multi-component induction measurements are more sensitive to horizontal resistivity compared to the vertical resistivity. Therefore we always prefer to invert sequentially for Rh and Rv. We use this approach in our new processing algorithm. After obtaining the two principal components $\widetilde{h}_{zz}^{p}$ and $\widetilde{h}_{xx}^{p}$ and relative dip and rotation angles, we invert for Rh and Rv. As we mentioned previously, the $\widetilde{h}_{zz}^{p}$ principal component depends only on horizontal resistivity, and $\widetilde{h}_{xx}^{p}$ depends on both Rh and Rv. This allows us to apply a sequential approach: first use $\widetilde{h}_{zz}^{p}$ and invert for Rh, then fix Rh and use $\widetilde{h}_{xx}^{p}$ to invert for Rv.

The particular algorithms for Rh and Rv inversions are described in detail in Rabinovich and Tabarovsky, 2001 and in Tabarovsky et. al., 2001.

Synthetic Data Example

We tested the new algorithm on a synthetic data set generated for a resistivity range typical for the Gulf of Mexico logging environment. In Figure 4 in the right track, we present the distribution of horizontal resistivities (red

color) and vertical resistivities (magenta). The left track shows formation dip and azimuth (red tadpoles), borehole deviation and azimuth (black tadpoles), relative dip (blue) and tool rotation (cyan). We intentionally have simulated a fast tool rotation of the tool to illustrate a severe data acquisition scenario. The main features of this model are presented below:

- GOM range of resistivities: Rh ~ 0.4-20 Ohm-m, Rv/Rh ~ 1-5;
- 170-m interval, 55 layers, includes thick isotropic layers;
- Borehole Deviation= 44° at 144° azimuth;
- Formation Dip= 15° at 150° azimuth, Relative Dip=59°;
- Fast Rotation: 360° per 45 ft;
- Borehole is not included in the model.

The results of the synthetic data test are presented in Figures 5, 6, and 7. The left track in Figure 5 shows true and recovered formation dip and azimuth (red and black tadpoles, correspondingly), borehole deviation (cyan), recovered relative dip (blue) and tool rotation (green). In the second track from the left, we present the distribution of true and recovered horizontal and vertical resistivities: red solid line – true Rh, solid magenta – true Rv, dashed blue – recovered Rh, dotted dark red – recovered Rv. We observe that the true and recovered formation dip and azimuth as well as the true and recovered Rh and Rv agree almost perfectly.

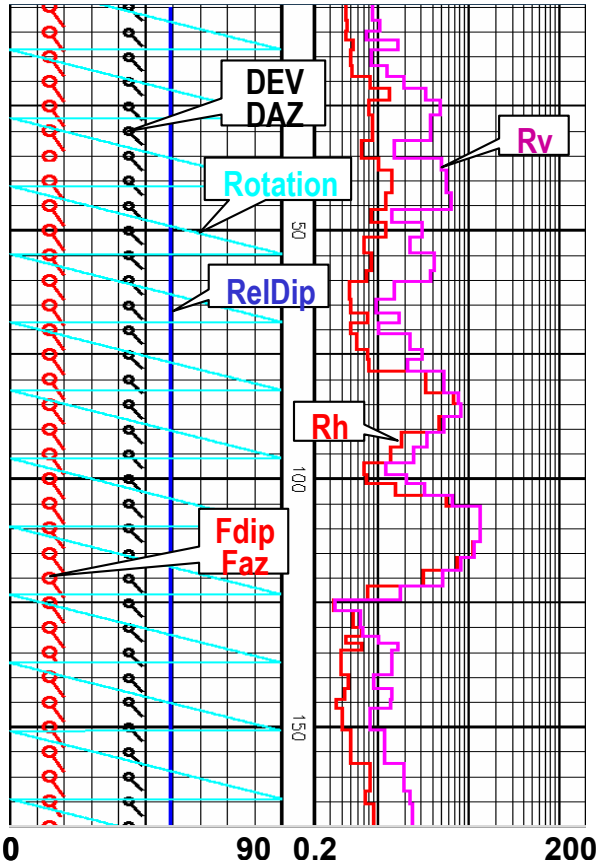

Fig. 4 *Synthetic model. A model generated for a resistivity range typical for the Gulf of Mexico.*

The right track in Figure 5 contains two pairs of the principal ZZp and XXp components on the shifted resistivity scale. Solid line curves represent the principal components obtained during least-square inversion for formation dip and azimuth: ZZp in black and XXp in blue. Dashed line curves depict synthetic principal components calculated during the second stage inversion for Rh and Rv: magenta – ZZp, green -XXp. The excellent match of the corresponding solid and dashed curves confirms the quality of the inversion for horizontal and vertical resistivity.

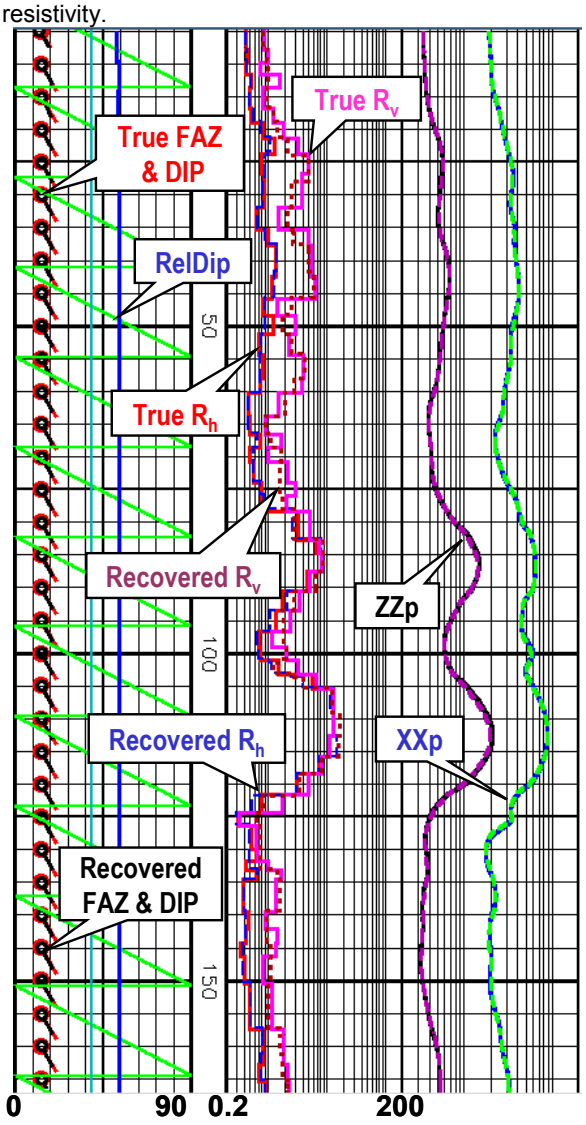

Fig. 5 *Recovered formation orientation and resistivities in synthetic model. The true and recovered formation dips (red and black tadpoles correspondingly) as well as true and recovered Rh and Rv (track in the middle) agree very well.*

In Figure 6 we show five measured (solid lines) and recovered (dashed lines) MFF components obtained during the first stage least square inversion for formation dip and azimuth. The almost perfect agreement of the

measured and synthetic curves confirms the high accuracy of the recovered formation dip and azimuth.

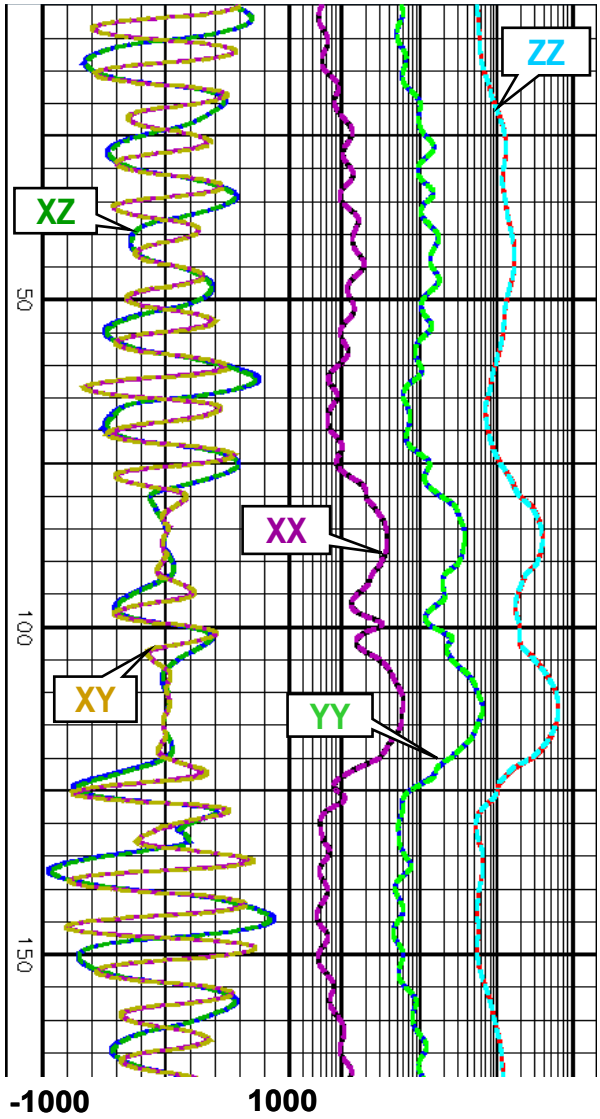

Fig. 6 *Data match for the measured components in synthetic model*

In Figure 7 we present the certainty maps obtained during the least-square inversion for formation dip and azimuth. Shown in the two panels are data inversion images: the left one shows the misfits for all possible formation dips when the formation azimuth is optimal (in this case it was 150°); and the right panel depicts the misfits for all formation azimuths when the formation dip is optimal (15°). The misfit is calculated using χ^2–norm and presented in the color-coded logarithmic scale ranging from 1 to 10, where 1 is the white color and 10 is the black color. We see that selecting the minimum misfit values (solid lines) we can accurately recover the true formation dips and azimuths (dashed lines).

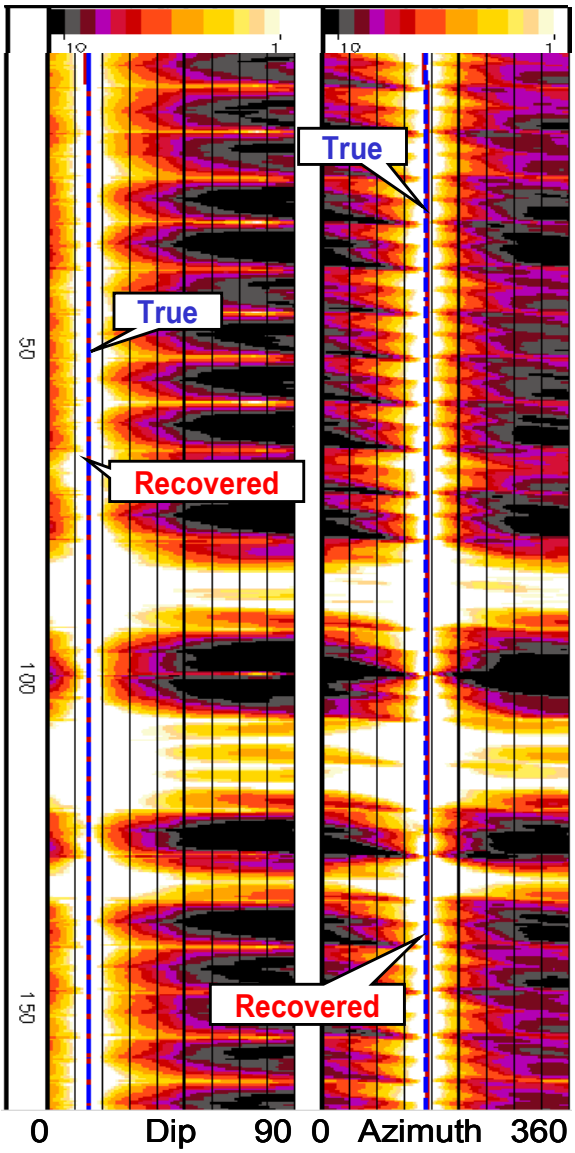

Fig. 7 *Images of the data certainty for the synthetic model. A left panel shows the misfits in color-coded logarithmic scale (1 to 10) for all possible formation dips when the formation azimuth is optimal. The right panel depicts the misfits for all possible formation azimuths when the formation dip is optimal. The width of the white bands indicates the uniqueness of the solution and the uncertainties in recovered formation dip and azimuth.*

These images clearly illustrate the data resolution and sensitivity to the formation dip and azimuth. For example, we observe that the minimum of the misfit is more distinctive (a white strip is narrower) when the anisotropy ratio increases. On the other hand all isotropic intervals (82-90 m, 107-118 m, 125-132 m) show no sensitivity to formation orientation. Accurate results in these isotropic intervals are only possible when relatively large windows (15 ft) used in the processing.

We should mention that these results were achieved using hands-off processing with three iterations and used minimal processing time.

Conclusions

We have developed a new processing technique for the multi-component induction instrument that, in addition to Rh and Rv resistivities, allows us to calculate the formation dip and azimuth. The main algorithmic ideas implemented in this technique are the following:

- Multi-frequency focusing removes the near-borehole effects and reduces the number of unknown principal components to two;
- Least-square inversion is applied to calculate the formation dip and azimuth using an over determined system of equations in the first stage of the processing;
- Sequential inversions for Rh and Rv are performed in the second stage using the recovered principal components and formation dip and azimuth.

Processing of the field and synthetic data confirms the validity and robustness of the new approach.

Acknowledgments

The authors wish to thank Baker Atlas for permission to publish this work. We appreciate many fruitful discussions with the project team members. We thank S. Dymmock for processing and interpreting the imaging data from Brazil. Special thanks to V. Mogilatov, E. Iomdina, J. Black, and O. Khan for their contribution in the software development, and to D. Georgi and K. Bush for editing this paper.

References

Klein, J., 1996. Saturation effects on electrical anisotropy, The Log Analyst, Jan-Feb, pp. 47-49.

Kriegshauser, B., Fanini, O., Forgang, S., Itskovich, G., Rabinovich, M., Tabarovsky, L., Yu, L., Epov, M. and van der Horst, M 2000. A new multi-component induction logging tool to resolve anisotropic formation, SPWLA 40th Annual Logging Symposium Transactions, Paper D.

Kriegshauser, B., Fanini, O., Yu, L., van der Horst, J., and van Popta, J., 2001, Improved shaly sand interpretation in highly deviated and horizontal wells using multicomponent induction log data, SPWLA 42nd Annual Logging Symposium Transactions, Paper S.

Mollison, R., Schoen, J., Fanini, O., Kriegshauser, B., Meyer, W., and Gupta, P., 1999. A model for hydrocarbon saturation determination from an orthogonal tensor relationship in thinly laminated anisotropic reservoirs, SPWLA 40th Annual Logging Symposium, Paper OO.

Mollison, R., Fanini, O., Kriegshauser, B., Yu, L., Ugueto, U., and van Popta, J., 2001. Impact of multi-component induction technology on a deepwater field turbidite sand hydrocarbon saturation evaluation: SPWLA 42nd Annual Logging Symposium, Paper T.

Oldenburg, D., 1994. Practical strategies for the solution of large scale electromagnetic inverse problems: Radio Science, **29**, 1081-1099.

Rabinovich, M., and Tabarovsky, L., 2001. Enhanced anisotropy from joint processing of multi-component and multi-arrays induction tools: Transactions of the SPWLA 42nd Annual Logging Symposium, paper HH.

Schoen, J., Mollison, R., and Georgi, D., 1999. Macroscopic electrical anisotropy of laminated reservoirs: a tensor resistivity saturation model, SPE Annual Technical Conference, SPE 56509.

Tabarovsky, L., and Epov, M., 1979. Geometric and frequency focusing for investigation of anisotropic layers, in Electromagnetic well logging, Nauka, Siberian Division, Acad. Sc. USSR.

Tabarovsky, L., and Rabinovich, M., 1996. High-speed 2-D inversion of induction logging data: Transactions of the SPWLA 37th Annual Logging Symposium, paper P.

Tabarovsky, L., and Rabinovich, M., 1998. Real-time 2-D inversion of induction logging data: Journal of Applied Geophysics **38** (1998) 251-275.

Tabarovsky, L., Epov, M., and Rabinovich, M., 2001. Measuring formation anisotropy using multi-frequency processing of transverse induction measurements, SPE 71706.

Tabarovsky, L., and Rabinovich, M., 2001. Determination of formation anisotropy using multi-frequency processing of induction measurements with transverse induction coils, US Patent US 6,574,562 B2.

Yu, L., Kriegshäuser, B., Wang, T., and Driskill, B., 2004, Real time processing of multicomponent induction tool data in highly deviated and horizontal wells: Transactions of the SPWLA 45th Annual Logging Symposium, paper ZZ.

Yu, L., Rabinovich, M., Tabarovsky, L., and Wang, T., 2003. The reduction of near zone effects on the multi-component induction logging tool, SPE 84097.